TECHNISCHE MECHANIK
European Journal of Engineering Mechanics
Diamond Open Access
journal homepage: www.ovgu.de/techmech

Tech. Mech., Vol. 46, Is. 1, (2026), 93–103
Received: 18.11.2025
Accepted: 21.01.2026
Available online: 16.02.2026

LES and DES of flow and ice accretion on wind turbine blades

Johan Revstedt[1]*, Robert-Zoltán Szász[1], and Stefan Ivanell[2]

[1] Lund University, Department of Energy Sciences, Ole Römersväg 1F, SE-223 63 Lund, Sweden
[2] Uppsala University, Department of Earth Sciences, Villavägen 16, 752 36, Uppsala, Sweden

Abstract: The aerodynamic effects of ice accretion on wind turbine blades has been studied using numerical methods. The ice accretion process on an aerofoil was simulated using RANS based simulations. The aerodynamic performance of the iced aerofoil was then investigated using several turbulence models, including both LES and DES. Aeroacoustic simulations using the Curle analogy were also performed. The results show that the shape of the ice has a profound influence on the lift and drag of the aerofoil and a small change in the ice shape can have a significant impact on the performance. Also, the choice of turbulence model is found to be important, with the results varying significantly between models. Both the geometry and the choise of tubulence model also have an influence on the noise propagation from the aerofoil.

Keywords: aerodynamic performance, ice accretion, LES, wind turbine

1 Introduction

During the past decade, a substantial amount of wind power capacity has been developed in cold climate regions. Driving factors for this development are low population densities, as well as favourable atmospheric conditions featuring low air densities and often higher average wind speeds than in more moderate climates. In recent years, particularly large developments took place in Inner Mongolia (China), Northern Scandinavia and Finland, as well as Canada (Wallenius and Lehtomäki, 2016). Despite the overall potential for wind power in cold-climate regions, the risk of blade icing poses a serious challenge for the operation of wind turbines in such areas. On the one hand, this relates to associated security issues such as ice throw. On the other hand, the aerodynamic degradation of the blades due to icing can bring about notable production losses as well as increased turbine loads. Today, about a quarter of the global installed wind energy capacity is expected to be prone to the risk of icing (Stoyanov and Nixon, 2020). In counties like Sweden, with more than 80% of the installed capacity in 2020 being located in the most northerly quarter of the country, even higher shares of the turbine fleet are situated in icing-affected regions (Badman and Tengblad, 2021). The modelling and forecasting of icing events and their impact on turbine performance and loads is therefore gaining importance for both planning and operation of wind farms.

Modelling the impact of icing on the blades of multi-megawatt wind turbines entails various coupled processes that need to be incorporated. The modelling challenge thus not only relates to the difficulties in modelling each individual process, but also in their connectivity and, consequently, the sensitivity of individual processes to the outputs of preceding modelling steps. Significant efforts have been made to investigate these processes including the meteorological forecasting of potential icing conditions, the modelling of ice accretion processes on airfoil sections (Bragg et al., 2005; Fu and Farzaneh, 2010; Ronsten et al., 2012), the prediction of airfoil degradation due to accumulated ice and, finally, the modelling of power and loads of the full turbine. While some work purely focused on one of the aforementioned involved processes, most studies seek to establish an entire *model chain* comprising several connected models, each for one respective process.

To date, the majority of studies with an engineering perspective typically start from a given time series of liquid water content (LWC), temperature and wind speed. Based on such a set of input variables the accretion of ice on the airfoil sections of the turbine blade can generally be modelled. The first studies of the impact of icing on airfoils date back to 1930's and originated in the aerospace community (Jones and Williams, 1936; Gulick, 1938). Over the past two decades various authors presented more specific studies on the accretion on wind turbine blades. Among these one may mention the work of Kangash et al. (2022) and Son and Kim (2020).

Due to the scale separation in time between the flow and ice accretion, a common approach is to compute the ice accretion and the flow around the ice accreted airfoils in separate stages. For the flow computations a common approach is to use simplified methods to reduce the computational efforts. For example, a potential flow solver is used in LEWICE (although there is a possibility to import flow fields from other solvers) (Wright, 2008), whereas the panel method is used in TURBICE (see e.g. Homola et al. (2010)). Recently, thanks to the increase in computational power and to the need to account for 3D effects, it is more and more common to solve the full set of Navier-Stokes equations (see e.g. Gori et al. (2015); Jin and Virk (2019); Prince Raj et al. (2020)). Droplet transport is commonly modeled either in an Eulerian (e.g. Prince Raj et al. (2020)) or Lagrangian (e.g. Szasz and Fuchs (2012); Szasz et al. (2016); Gori et al. (2015)) framework.

In the case of rime ice conditions one can assume that all droplets hitting the surface freeze instantaneously, thus there is no need for heat transfer computations. The amount of droplets hitting the surface is determined explicitly or specified via the collection efficiency, depending if a lagrangian or eulerian model is used for droplet transport. To model glaze ice, the most common

* E-mail address: johan.revstedt@energy.lth.se
doi: 10.24352/UB.OVGU-2026-010

approach is to compute 1D heat transfer problems based on the so-called Stefan's problem formulated for aeronautical applications by Messinger in 1953 and further improved by Myers in 2001 (see e.g. Gori et al. (2015)).
In the case of severe icing conditions the ice structures formed on the surfaces may significantly change the flow topology. In order to account for such changes, a common approach is to divide the time interval of the entire icing event in sub-intervals. During each sub-interval the geometry is considered constant. Before the next time interval is computed, the surface (and the mesh used for the flow computations) is updated to account for the ice accreted during the previous interval. Such a multi-step approach is used e.g. in Gori et al. (2015). A sensitivity study to physical and modeling parameters affecting airfoil icing is shown in Prince Raj et al. (2020).
The modified lift and drag curves of the airfoil sections resulting from the ice accretion computations can then be employed in an aerodynamic model of the wind turbine, typically based on the blade element momentum (BEM) method (Hansen, 2008). Homola et al. (2012), for instance, employed such a model chain to investigate the impact of a generic one hour icing event on the NREL 5MW reference turbine (Jonkman et al., 2009). A similar study was conducted by Etemaddar et al. (2014). Again imposing generic constant icing events, the authors investigated the sensitivity of the icing degradation to different meteorological and operational conditions. Later, Zanon et al. (2018) also employed the aforementioned models but not in a sequential but in a weakly coupled manner. More specifically, the BEM approach provided the instantaneous rotational speed of the turbine during the icing event which allowed for an adaptation of the inflow conditions in the RANS-based accretion simulation. Others replaced the plain BEM model with a coupled aero-elastic solver in order to investigate the impact of icing on the structural dynamics of the turbine (Rissanen et al., 2016; Gantasala et al., 2016, 2019).
Hence, the overarching aim of this project is building the model chain for meteorological simulations through ice accretion simulations of the wind turbine blades to simulate the performance of an ice accreted turbine. The particular focus of this paper is the sensitivity of the middle link in the chain, i.e. simulations of the ice build-up and the aerodynamic performance of a blade section. One of the underlying reasons for performing this study is to investigate the robustness of our model for ice accretion and the effects that it might have on obtaining the aerodynamic performance of a wind turbine blade. An important factor in the overall robustness is also the choice of turbulence model and its consequences for the results.

2 Method

We are considering incompressible flow around an aerofoil, which is governed by the incompressible Navier-Stokes equations. Two kinds of simulation are performed, ice accretion simulations mainly performed using RANS models and simulations to acquire the aerodynamic forces where we employ LES and DES models. The methods used for the different simulations are given below.

2.1 Ice accretion simulations

In this work we assume that only rime ice is formed, i.e. the air contains super cooled water droplets that will freeze instantly in contact with the wing section. To model this, we represent the liquid water droplets using a statistical Lagrangian particle tracking (LPT) method. Each motion of each droplet parcel is described by

$$\frac{\mathrm{d}\boldsymbol{u}_j}{\mathrm{d}t} = \left(\rho_{\mathrm{air}} - \rho_d\right) g \frac{\pi d^3}{6} + \boldsymbol{f}_j \tag{1}$$

i.e. we only account for drag and gravity forces. Since the droplets are very small ($d = 27\mu$m) we neglect their influence on the air, i.e. one-way coupling. Effects of turbulence on the droplet motion are accounted for using a statistical particle dispersion model in which both the direction and magnitude are randomised and for the latter related to the local magnitude of turbulent kinetic energy, i.e. what is commonly known as a random walk model. The ice accretion simulations are performed using OpenFOAM 4.1 in combination with an in-house tool for morphing the aerofoil surface based on the amount of ice accreted. The simulations are, in general, performed in several steps, alternating between generating a flow field, calculating the ice accretion and morphing the surface. Details within these steps may vary depending on simulation strategy (i.e. choice of turbulence model etc.). We have found that an efficient approach to create the iced aerofoil shape is to first create a statistically stationary flow field using a RANS simulation. Thereafter, the LPT is performed using this steady flow field and we account only for particle drag force and turbulent dispersion in the resulting differential equation of each droplet parcel. The turbulent dispersion is done with a stochastic model (a.k.a random walk). Each parcel of Lagrangian particles that impacts the aerofoil surface is registered. Since we are only considering rime ice, a droplet impacting the surface is considered to freeze immediately. It should be noted here that the time scale of the flow and the ice accretion differ substantially, with the icing time scale being much longer. To increase the computational efficiency we have therefore shortened the time scale by increasing the LWC artificially. Our previous investigations show that it is possible to decrease the time scale of ice accretion by a factor 1000, i.e. one hour of ice accretion is represented by 3.6 seconds of flow time. Following each hour of ice build-up the simulation is halted and the nodes of the aerofoil surface mesh are moved in accordance with the amount of ice accreted in each cell ensuring that the ice mass is conserved. Thereafter a new computational mesh is generated using *snappyHexMesh* and the aforementioned simulation steps are repeated. An example of the mesh of morphed aerofoils are depicted in Figure 1.

2.2 Surface smoothing

The ice distribution is smoothed over the airfoil surface. This step is motivated by the fact, that even if the length of the LPT computations is long enough to achieve a statistically converged ice distribution, depending on the mesh resolution used to discretise the airfoil, there might be small cells with no ice accreted, leading to physically irregular shape of the ice accreted surface.

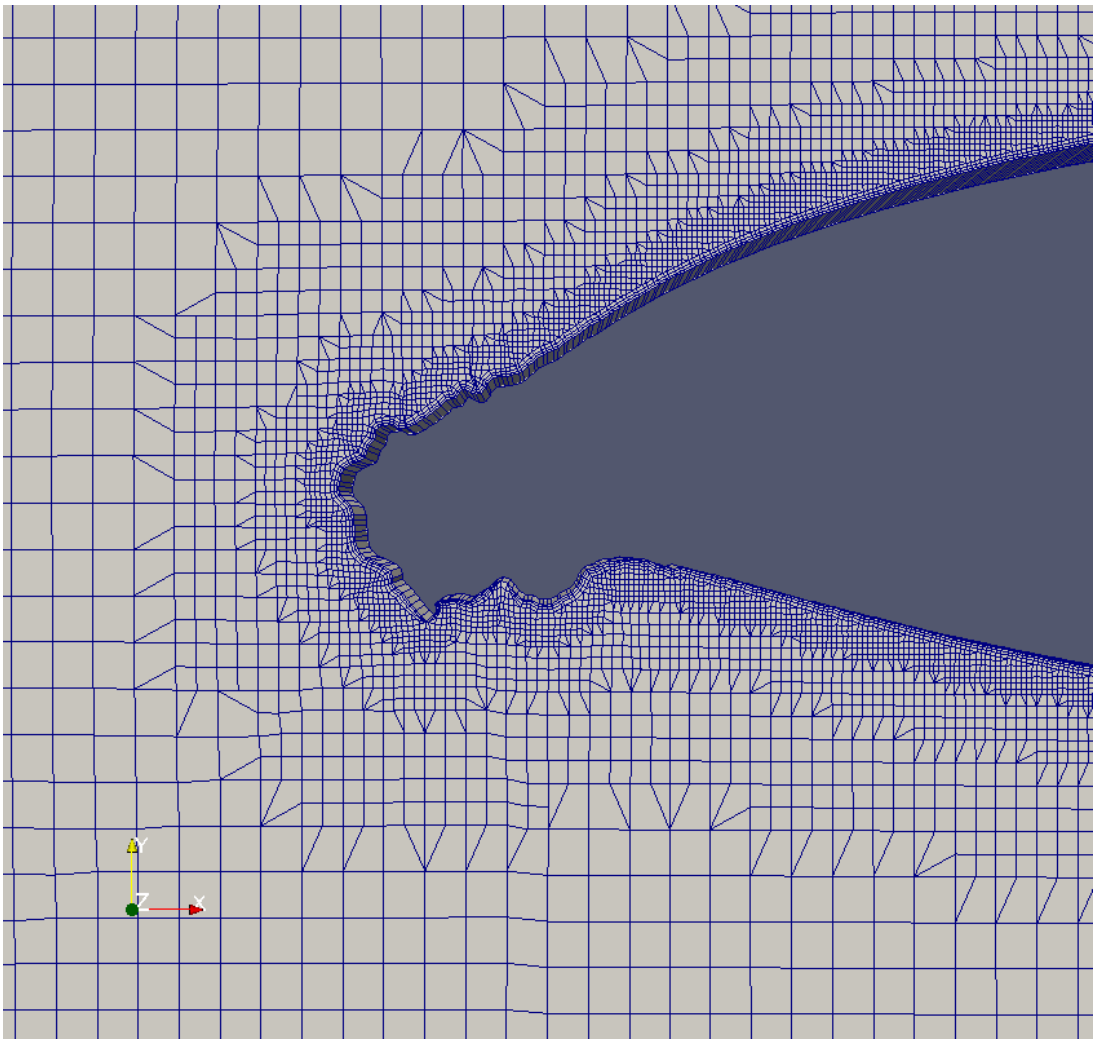

Fig. 1: Example of a mesh from the ice accretion simulations

The smoothing is done by transferring the information about the amount of accreted ice from cell centers to cell vertices and vice versa. The amount of accreted ice is stored during the CFD simulations in cell centers. The smoothing operates on the mass surface density, m_i:

$$m_i = M_i / A_i \tag{2}$$

where M_i is the amount of ice accreted in cell i and A_i is the area of cell i. Assuming that the amount of ice accreted in a cell contributes equally to the three vertices of the cell, the vertex values are computed as:

$$m_v = \sum_{i=1}^{Nt_v} m_i / 3 \tag{3}$$

In the second step the information is transferred back to the cell centers:

$$m_i = \sum_{v=1}^{3} m_v / Nt_v \tag{4}$$

where Nt_v is the number of triangles (cells) sharing vertex v. The effect of smoothing is increasing with increasing number of loops applying Eqs. (3) and (4). After smoothing, the accreted mass in each cell is updated as:

$$M_i = m_i \, A_i \tag{5}$$

2.3 Turbulence modeling

In the ice accretion phase of the simulations we are using the SST k-ω model (Menter, 1994). To study the aerodynamic performance of the iced aerofoils we also use LES and DES models. The LES approaches considered are the WALE model (Nicoud and Ducros, 1999) and the one equation eddy model (Yoshizawa, 1986). The hybrid model considered is the IDDES based on the Spalart-Allmaras model (Spalart et al., 1997).

2.4 Aeroacoustic modeling

The aeroacoustic simulations are performed in OpenFOAM v2206 using the Curle analogy (Curle, 1955).

3 Computational set-up

The case considered in this study has the same specifications as one of the rime ice cases in the wind tunnel study by Hochart et al. (2008) (their case 5).
The computational domain is outlined in Figure 2. The aerofoil shape is a NACA 63-415 which is placed 6 chord lengths (c) from the inlet, the distance to the outlet from the leading edge is $10c$ and the upper and lower boundaries are placed $6c$ from the aerofoil. The width of the aerofoil is $0.4c$. The chord length is 0.2m and the wind speed is 36m/s which corresponds to a Reynolds number of $\mathrm{Re_c} = 475,000$. The meshes used are hexahedral with unstructured refinements created using *snappyHexMesh*. The number of cells is about $2.2 \cdot 10^6$ in the LES cases and somewhat less for the RANS based simulation ($1.5 \cdot 10^6$), but also varies slightly between cases due to the differences in ice shape. The cell size in the refinement closest to the wing section is $c/320$. However, wherever possible, it is further refined in the surface-normal direction. A typical mesh layout is shown in Figure 3. The small difference in mesh resolution between the RANS and LES is mainly due to that the RANS mesh resolution in the streamwise and spanwise directions close to the aerofoil surface was seen with the intention to properly resolve the ice accretion process and the resulting surface. To get an indication of the mesh sensitivity, we compare the lift coefficient for the case of $\alpha = 7^o$ with resolutions $c/320$ and $c/160$, respectively. For the RANS based simulations, the difference is then about 5 %, while it is about 20% for the one equation eddy model. Considering the wall normal resolution, y^+ varies between 0.025 and 9.0 with an average value of 1.7 for the one equation eddy model, while for the RANS simulations the average value is about 10. The velocity and the variables for the turbulence are set as constant values at the inlet and using the Neumann conditions at the outlet. The pressure is defined as constant at the outlet. The other outer boundaries of the domain specified using the slip condition. On the aerofoil we use no-slip

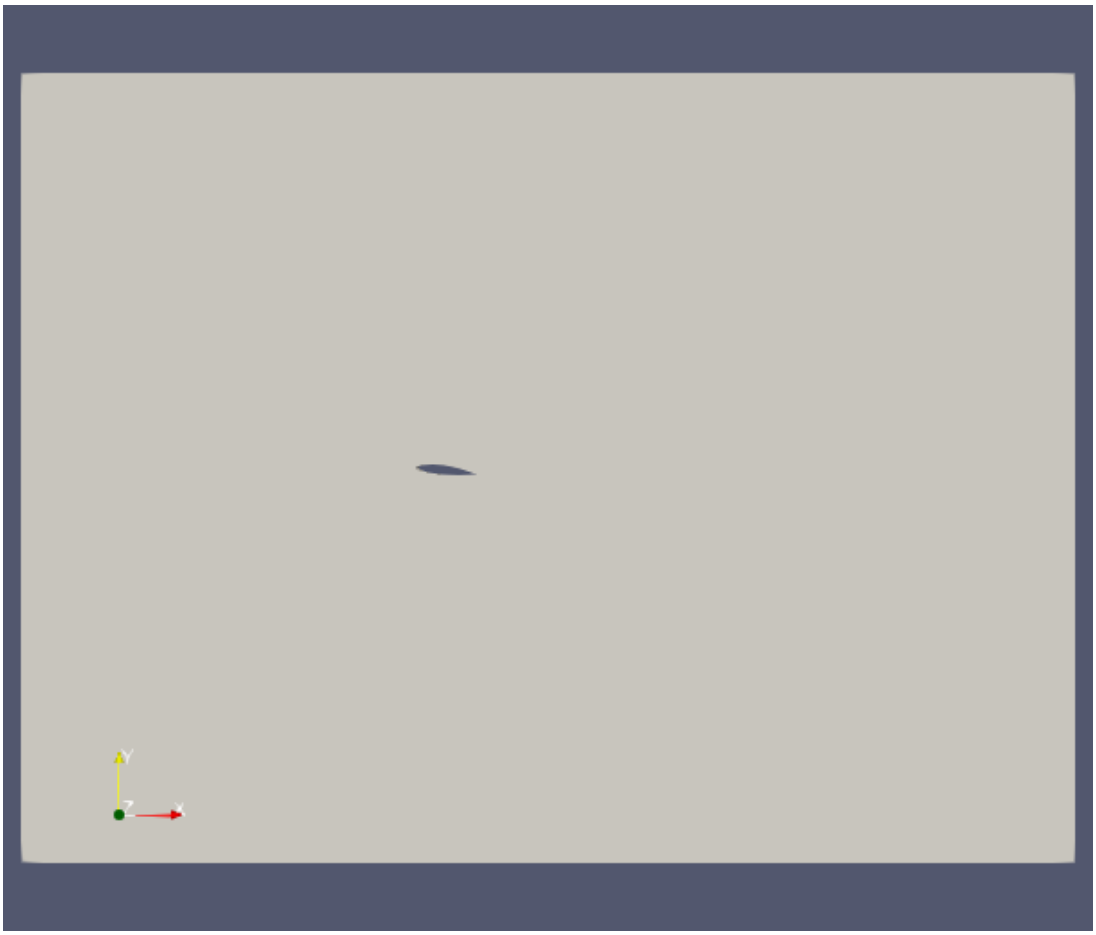

Fig. 2: Computational domain

conditions. For the ice accretion simulations a RANS model is used (SST k-ω model (Menter, 1994)).

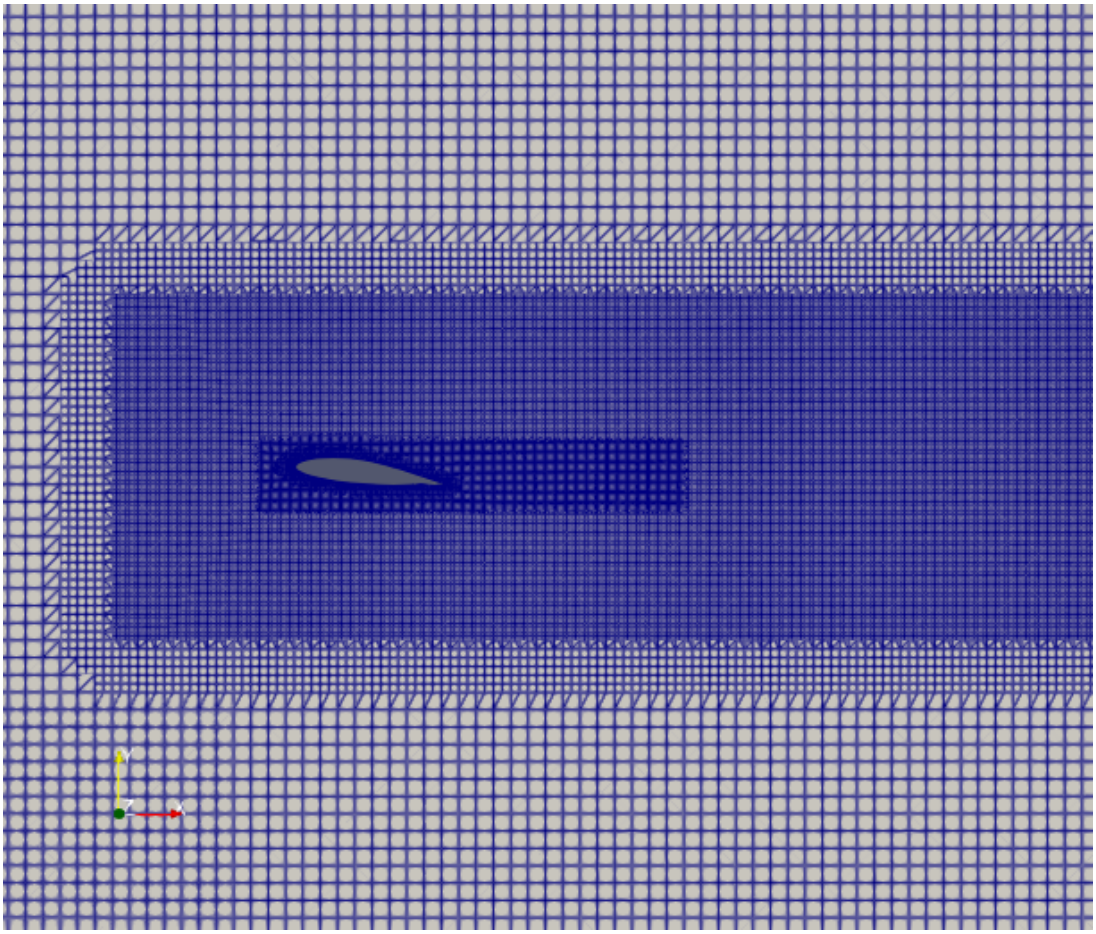

Fig. 3: Mesh configuration, showing the local refinements around the aerofoil

In the accretion based simulations the following steps are taken. First a flow field is created using a steady state simulation. The particle simulation is then run using this ”frozen” flow field. After a certain time the simulation is stopped and the aerofoil geometry is updated based on the number of droplets on the surface using the method outlined in Section 2.2. Here we use either 200 or 500 smoothing steps. A new mesh is then generated and a new flow field simulated. This is repeated until the required icing time is achieved. It should be noted that in reality the time scales for the flow and for the ice accretion process differ by several orders of magnitude. The ice accretion process has therefore been accelerated by a factor 1000 in order to reach reasonable simulation times. This is done by increasing the number of droplets in each parcel. The total ice accretion time in Hochart's wind tunnel experiment was 11.8 minutes, which corresponds to 0.708 s in our simulation. This was divided into 24 simulations of 0.0295 s each with morphing and smoothing of the geometry in between simulation.
The study of the aerodynamic performance of the iced aerofoil is performed using both geometries originating from using 200 and 500 smoothing steps respectively. Most of the simulations here are performed using the one equation eddy model by Yoshizawa (1986), however, in some cases we have also used the WALE model, the IDDES model and the SST model for comparison. In these simulations the angle of attack, α, has been varied between 2 and 12 degrees.
The RANS simulations are performed using SIMPLE approach (*simpleFoam*). The convective terms are discretised using a bounded second order upwind scheme and for the diffusive terms a second order central scheme is used. In the LES a bounded central scheme is used for the convective terms and we use the *pimpleFoam* solver instead.

4 Results

4.1 Ice mass and profiles

As can be seen from Table 1 our simulations slightly overestimates the amount of ice accreted on the surface compared to Hochart et al. (2008). As can also be observed, the difference in ice mass between our two cases is also fairly small. Turning our attention to how the ice mass is distributed on the surface we can see from Figure 4 that the iced profiles from the two simulations are very similar. Most of the ice is located close to the leading edge of the aerofoil with also a fairly large amount accreted on the lower side, while the upper side is almost clean. This coincides fairly well with the measured profile (red dotted line in Figure 4). However, there are some important features missing in the simulation. The most pronounced of these are the horn shape created on the upper side of the aerofoil and the waviness in the lower side. These features, especially the horn, might have a significant impact on the aerodynamic performance of the aerofoil.

Tab. 1: Accreted ice mass for the two levels of smoothing also comparing to the data of Hochart et al. (2008) of 0.182 kg/m

Smooth steps	Accreted mass [kg/m]	Difference compared to Hochart et al. (2008) in %
200	0.190	4.4
500	0.198	8.8

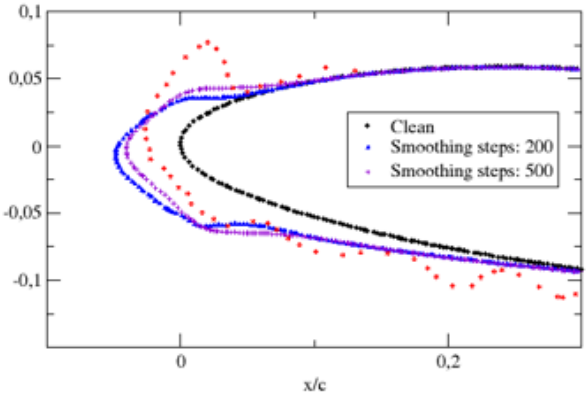

Fig. 4: Aerofoil shape with ice at midspan for different levels of smoothing during the accretion process.

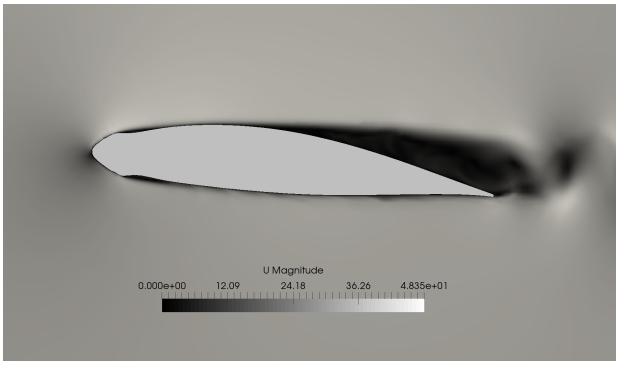

Fig. 5: Velocity field at $\alpha = 7$ deg.

4.2 Aerodynamic forces

One would expect that an aerofoil subjected to ice accretion would perform worse aerodynamically than a clean one. Considering Figure 6 this is indeed the case with two exceptions. For almost all angles of attack α the lift coefficient is lower and the drag coefficient is higher for the iced aerofoils. However, in two cases we locally observe an opposite trend. For the case with 200 smoothing steps in the ice accretion simulations (SM200) the performance is instead significantly better at $\alpha = 9^o$ and for SM500 similar results are found at $\alpha = 7^o$. In an effort to explain this behaviour let us consider snapshots of the speed at the four cases of interest. First consider the situation at $\alpha = 7^o$ shown in Figure 7. In the SM200 case the flow stays attached up to about half the chord length, where after a laminar separation occurs causing a fairly large wake. However, for SM500 the ice layer is at a slightly different angle causing a separation close to the leading edge with an almost immediate reattachment and the flow stays attached all the way to the trailing edge, with the boundary layer becoming turbulent at about 60% of the chord. From this the locally improved performance of the SM500 is obvious. Looking instead at $\alpha = 9^o$ the situation is slightly different (Figure 8). Here the SM200 geometry behaves almost identically to what we observed for SM500 at $\alpha = 7^o$, while the SM500 here displays a strong leading edge separation deteriorating the aerodynamic performance.

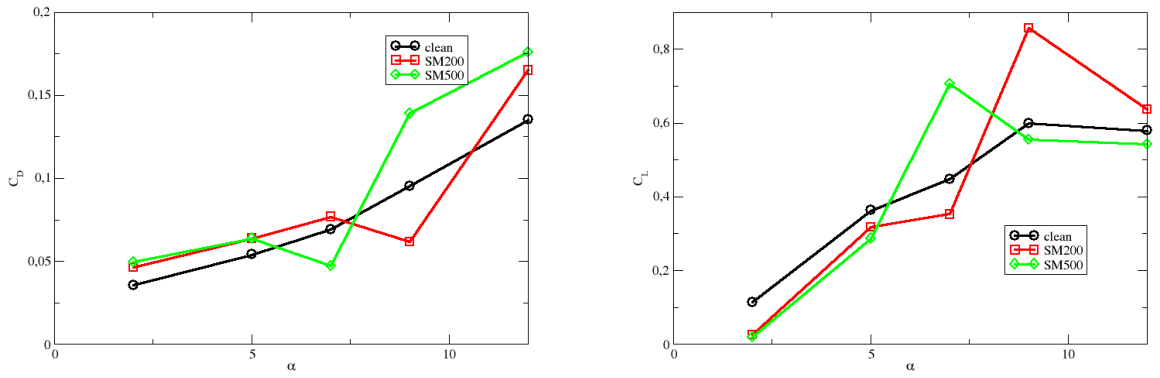

Fig. 6: Lift and drag coefficient as a function of angle of attack of the iced aerofoils compared to the clean one. All simulations performed using the one-equation eddy model

4.3 Influence of turbulence model

It might also be of interest to investigate the sensitivity to turbulence model for the ice-accreted aerofoil. We start by considering the case $\alpha = 7^o$, since that is the angle of attack used by Hochart et al. (2008) and the smoothing case SM200.
As can be seen from Table 2 the variation in drag and lift between turbulence models is significant. Nevertheless, all these models

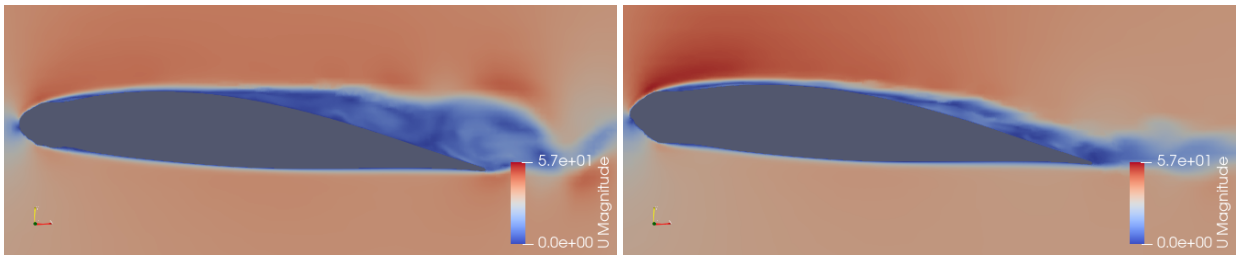

Fig. 7: Snapshot of the speed for SM200 (top) and SM500 (bottom) for $\alpha = 7^o$. All simulations performed using the one-equation eddy model

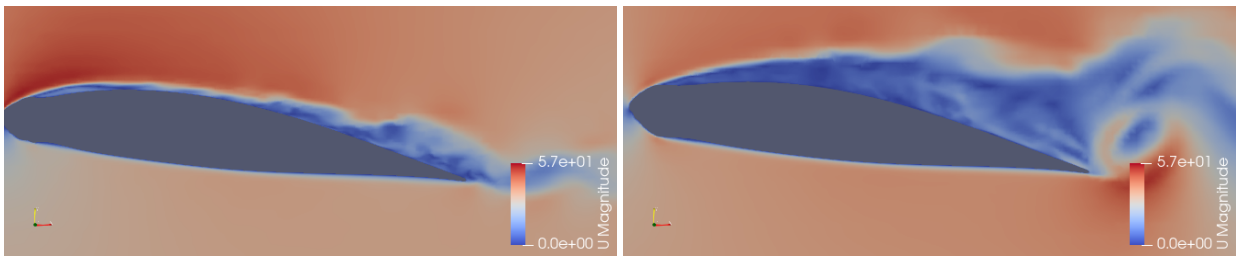

Fig. 8: Snapshot of the speed for SM200 (top) and SM500 (bottom) for $\alpha = 9^o$. All simulations performed using the one-equation eddy model

show an increase in drag and a decrease in lift compared to a clean aerofoil simulated with the same turbulence model and instead tabulating the ratios of lift and drag coefficients shows a slightly different picture, as is seen in Table 2.

A closer look at the aerodymanic forces from the SST k-ω and WALE models in Figures 9 and 10 reveals that these are quite similar in results both concerning trends and values. Neither exhibits the strong variations in lift and drag experienced at $\alpha = 7^o$ and $\alpha = 9^o$ for the one-equation eddy model. However this does by no means indicate that the RANS simulations are insensitive to variations in the iced geometry. Figure 9 clearly shows a difference in forces for all angles of attack instead of the localized effect present in the one-equation eddy simulations. Snapshots of the velocity fields (Figure 11) can help us explain the difference in forces between the one-equation eddy and WALE models. It is evident from Figure 11 that the one-equation eddy model predicts a much earlier separation for almost all angles of attack which leads to differences in the boundary layer turbulence and

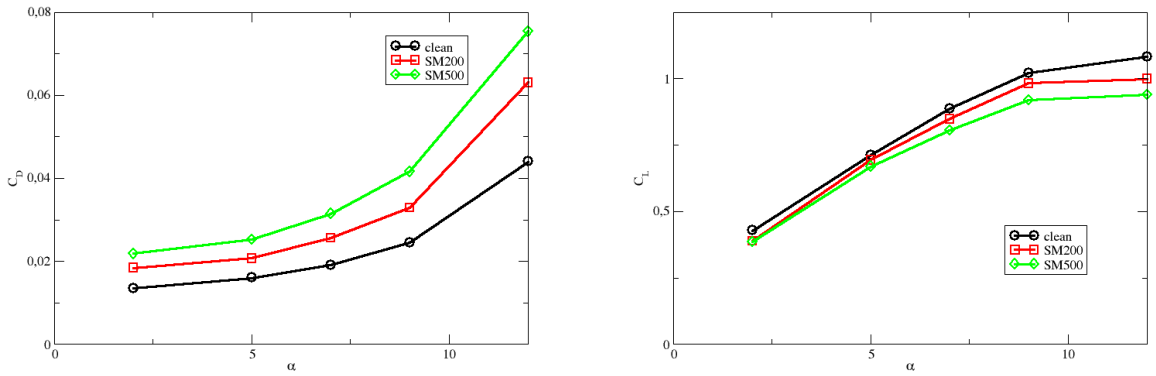

Fig. 9: Lift and drag coefficient as a function of angle of attack of the iced aerofoils compare to the clean one. All simulations performed using the SST k-ω model.

Tab. 2: Lift and drag coefficients for $\alpha = 7^o$, SM200 for various turbulence models. To be compared with the results of Hochart et al. (2008): $C_L = 0.491$, $C_D = 0.064$

Model	C_D	C_L
One equation eddy	0.078	0.360
WALE	0.021	0.808
IDDES	0.038	0.449
SST k-ω	0.026	0.850

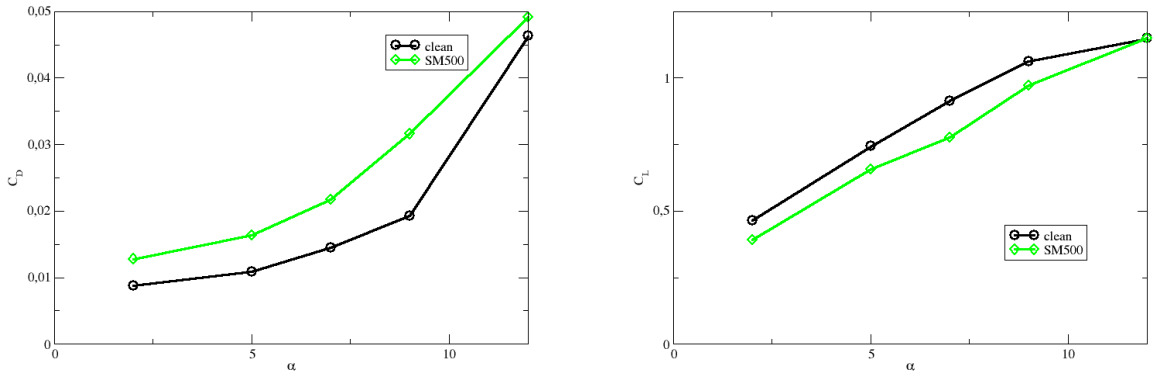

Fig. 10: Lift and drag coefficient as a function of angle of attack of the iced aerofoils compare to the clean one. All simulations performed using the WALE model.

Tab. 3: Ratios between lift and drag coefficients for an ice accreted and a clean aerofoil at $\alpha = 7^o$, SM200 for various turbulence models.

Model	$C_{\mathrm{D,ice}}/C_{\mathrm{D,cl}}$	$C_{\mathrm{L,ice}}/C_{\mathrm{L,cl}}$
One equation eddy	1.13	0.80
WALE	1.44	0.88
IDDES	1.66	0.66
SST k-ω	1.35	0.96

wake structure between the two sub-grid scale models and in turn clearly explains the higher drag and lower lift observed in the one-equation eddy model.

4.4 Noise emissions

Since the flow fields and hence also the aeodynamic forces show differences depending on the smoothing of the surface and the choice of turbulence model one might expect to see differences in the noise emissions as well. We have therefore used the Curle analogy (Curle, 1955) to study the noise at a point located some distance from the aerofoil. As can be seen from Figure 12, using the one equation eddy model actually the noise decreased for thee iced geometries compared to the clean one. Furthermore the SM500 case gives a significantly stronger decrease and broader peak of the main noise frequency, which can be explained by the differences we observe in wake structure in Figure 7. For the WALE simulations the difference is much less pronounced and very similar to what we find for the SM500 case with the one-equation eddy model.

5 Summary

Predicting the aerodynamic performance of an aerofoil subjected to ice accretion is a complex task. We have shown that slight differences in the iced geometry can have an enormous impact on the outcome at certain angles of attack, even showing improved performance. Comparing the different turbulence models used we can conclude that none of them are close to matching the data from Hochart et al. (2008). It would seem that the one-equation eddy model does a decent job but that model significantly under-predicts the lift on the clean profile. This puts its suitability for use in this Reynolds number range in question. One should also mention that we have not taken into account the effects of surface roughness the ice generates beyond what we can resolve in our mesh. Our earlier studies (not yet published) indicate that also adding surface roughness to a RANS simulation of an iced aerofoil significantly alters the aerodynamic performance.

Acknowledgments

The financial support for this work from the Swedish Energy Agency, project no. 47053-1, is gratefully acknowledged. Computational resources were provided by the centre for scientific and engineering calculations (LUNARC) at Lund University.

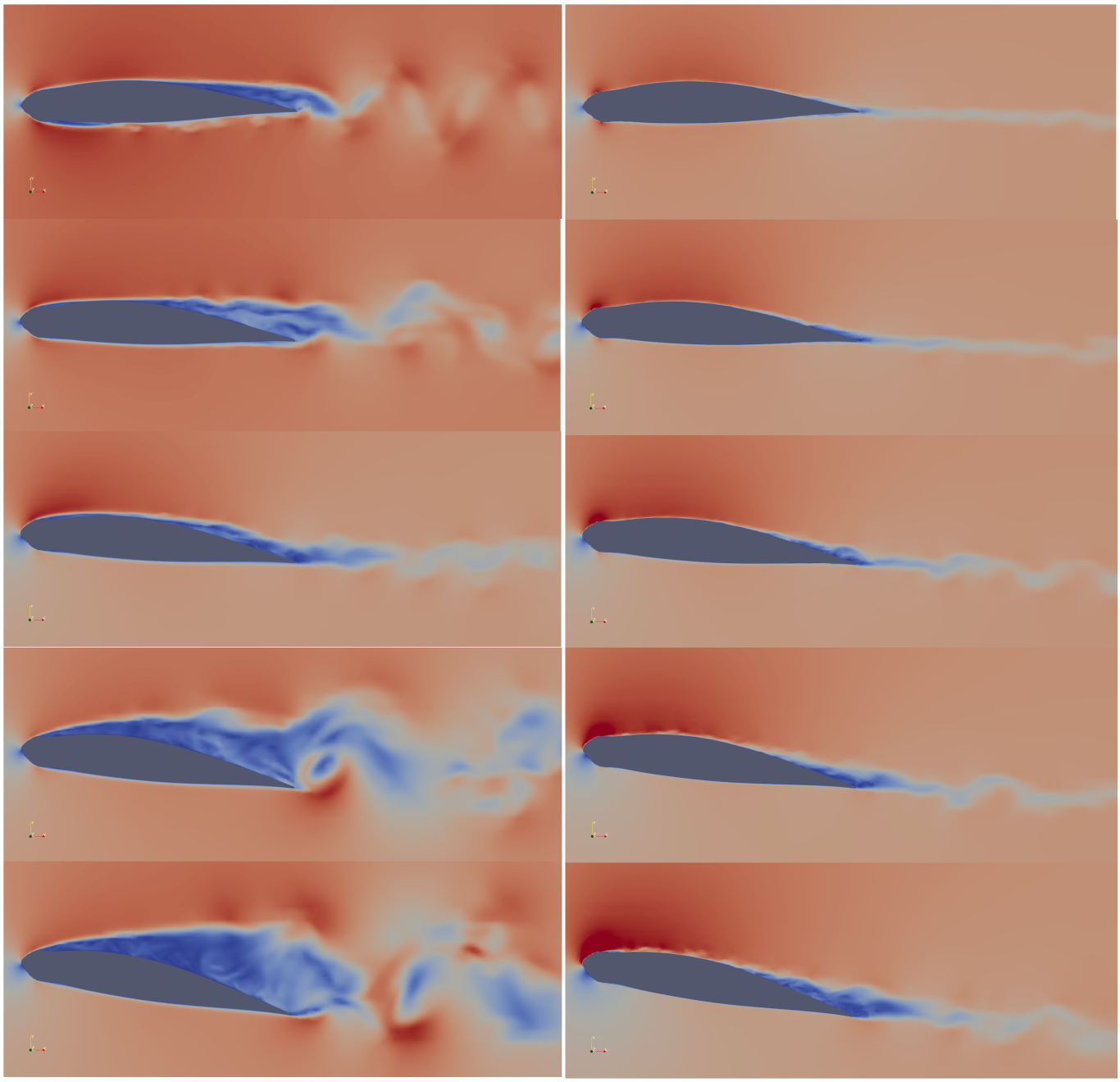

Fig. 11: Snapshots of velocity fields from $\alpha = 2^o$ (top) to $\alpha = 12^o$ (bottom. To the left is the one-equation eddy model and to the

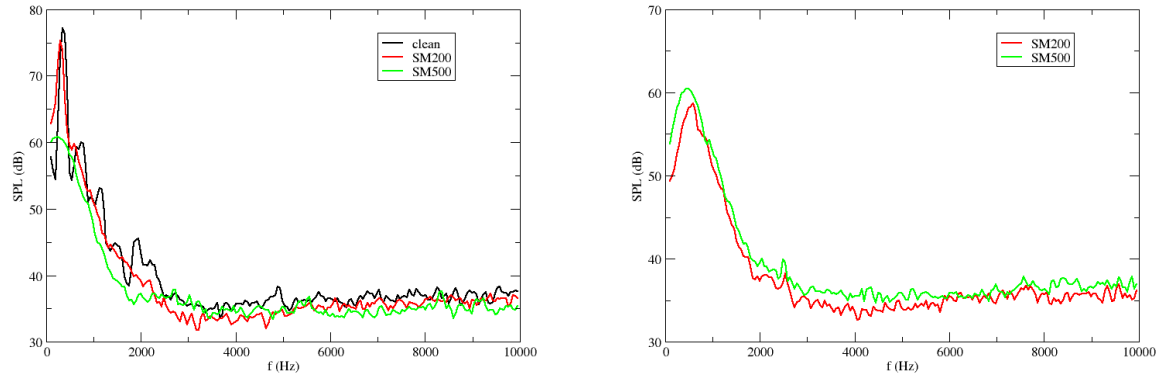

Fig. 12: Sound pressure level at the observation point 3 chord lengths above the trailing edge of the aerofoil for $\alpha = 7^o$. Above is the one-equation eddy model and below the WALE model.

References

D. Badman and Y. Tengblad. Roadmap 2040Wind power: Combating climate change and improving competitiveness. Technical report, Swedish Wind Energy Association, 2021.

M. B. Bragg, A. P. Broeren, and L. A. Blumenthal. Iced-airfoil aerodynamics. *Progress in Aerospace Sciences*, 41(5):323–362, July 2005. ISSN 03760421. doi: 10.1016/j.paerosci.2005.07.001.

N. Curle. The influence of solid boundaries upon aerodynamic sound. *Proc. of the Royal Society of London. Series A. Mathematical and Physical Sciences*, 231:505–514, 1955.

M. Etemaddar, M. O. L. Hansen, and T. Moan. Wind turbine aerodynamic response under atmospheric icing conditions. *Wind Energy*, 17(2):241–265, 2014.

P. Fu and M. Farzaneh. A CFD approach for modeling the rime-ice accretion process on a horizontal-axis wind turbine. *Journal of Wind Engineering and Industrial Aerodynamics*, 98(4-5):181–188, 2010.

S. Gantasala, J.-C. Luneno, and J.-O. Aidanpää. Influence of Icing on the Modal Behavior of Wind Turbine Blades. *Energies*, 9 (11):862, November 2016.

S. Gantasala, N. Tabatabaei, M. Cervantes, and J.-O. Aidanpää. Numerical Investigation of the Aeroelastic Behavior of a Wind Turbine with Iced Blades. *Energies*, 12(12):2422, January 2019.

G. Gori, M. Zocca, M. Garabelli, A. Guardone, and G. Quaranta. PoliMIce: A simulation framework for three-dimensional ice accretion. *Applied Mathematics and Computation*, 267:96–107, sep 2015.

B. G. Gulick. Effect of simulated iced formation on the aerodynamic characteristics of an airfoil. Technical Report R.N. NACA-Wr.L-292, NACA, 1938.

M. O. L. Hansen. *Aerodynamics of Wind Turbines*. London, UK: Earthscan, 2008.

C. Hochart, G. Fortin, J. Perron, and A. Ilinca. Wind turbine performance under icing conditions. *Wind Energy*, 11:319–333, 2008.

M. C. Homola, M. S. Virk, T. Wallenius, P. J. Nicklasson, and P. A. Sundsbø. Effect of atmospheric temperature and droplet size variation on ice accretion of wind turbine blades. *Journal of Wind Engineering and Industrial Aerodynamics*, 98(12):724–729, 2010.

M. C. Homola, M. S. Virk, P. J. Nicklasson, and P. A. Sundsbø. Performance losses due to ice accretion for a 5 MW wind turbine. *Wind Energy*, 15(3):379–389, 2012.

J. Y. Jin and M. S. Virk. Study of ice accretion and icing effects on aerodynamic characteristics of DU96 wind turbine blade profile. *Cold Regions Science and Technology*, 160(September 2018):119–127, apr 2019. ISSN 0165232X.

R. Jones and D. Williams. The effect of surface roughness of the characteristics of the airfoils NACA 0012 and RAF 34. Technical Report Report No.1708, British ARC, 1936.

J. Jonkman, S. Butterfield, W. Musial, and G. Scott. Definition of a 5-MW Reference Wind Turbine for Offshore System Development. Technical Report NREL/TP-500-38060, NREL, 2009.

A. Kangash, M. S. Virk, and P. Maryandyshev. Numerical study of icing impact on the performance of pitch-regulated large wind turbine. *Wind Engineering*, 47(2), 2022.

F. R. Menter. Two-equation eddy-viscosity turbulence models for engineering applications. *AIAA Journal*, 32:1598–1605, 1994.

F. Nicoud and F. Ducros. Subgrid-scale stress modelling based on the square of the velocity gradient tensor. *Flow Turbulence and Combustion*, 62(3):183–200, 1999.

L. Prince Raj, K. Yee, and R. S. Myong. Sensitivity of ice accretion and aerodynamic performance degradation to critical physical and modeling parameters affecting airfoil icing. *Aerospace Science and Technology*, 98:105659, mar 2020. ISSN 12709638.

S. Rissanen, V. Lehtomäki, J. Wennerkoski, M. Wadham-Gagnon, and K. Sandel. Modelling load and vibrations due to iced turbine operation. *Wind Engineering*, 40(3):293–303, June 2016.

G. Ronsten, T. Wallenius, M. Hulkkonen, I. Baring-Gould, R. Cattin, M. Durstewitz, A. Krenn, T. Laakso, A. Lacroix, L. Tallhaug, Ö. Byrkjedal, and E. Peltola. State-of-the-Art of Wind Energy in Cold Climates. Technical report, IEA Wind Task 19, 2012.

C. Son and T. Kim. Development of an icing simulation code for rotating wind turbines. *Journal of Wind Engineering & Industrial Aerodynamics*, 203:104239, 2020.

P. Spalart, W. Jou, and M. Strelets. Comments on the feasibility of les for wings, and on hybrid RANS/LES approach. In C. Liu and Z. Liu, editors, *Proceedings of First AFOSR International Conference on DNS/LES*, 1997.

D. B. Stoyanov and J. D. Nixon. Alternative operational strategies for wind turbines in cold climates. *Renewable Energy*, 145: 2694–2706, January 2020.

R.-Z. Szasz and L. Fuchs. Numerical modeling of ice accretion on a wing section. In J. Vad, editor, *Proceedings of the Conference on Modelling Fluid Flow*, pages 292–298, 2012.

R.-Z. Szasz, M. Ronnfors, and J. Revstedt. Influence of ice accretion on the noise generated by an airfoil section. *International Journal of Heat and Fluid Flow*, 62:83–92, 2016.

T. Wallenius and V. Lehtomäki. Overview of cold climate wind energy: Challenges, solutions, and future needs. *WIREs Energy and Environment*, 5(2):128–135, 2016.

W. Wright. User ' s Manual for LEWICE Version 3 . 2. Technical Report NASA/CR–2008-214255, NASA, 2008.

A. Yoshizawa. Statistical theory for compressible turbulent shear flows, with the application to subgrid modeling. *Physics of Fluids*, 29(7):2152–2164, 1986.

A. Zanon, M. De Gennaro, and H. Kühnelt. Wind energy harnessing of the NREL 5 MW reference wind turbine in icing conditions under different operational strategies. *Renewable Energy*, 115:760–772, 2018.